Numerical Simulation of Liquid Nitrogen Chilldown of a Vertical Tube

Samuel Darr[1], Hong Hu[2], Reid Schaeffer[3], and Jacob Chung[4]
Department of Mechanical and Aerospace Engineering, University of Florida, FL, 32611, USA

Jason Hartwig[5]
NASA Glenn Research Center at Lewis Field, Cleveland, OH, 44135, USA

Alok Majumdar[6]
NASA Marshall Spaceflight Center, Huntsville, AL, 35811, USA

This paper presents the results of a one-dimensional numerical simulation of the transient chilldown of a vertical stainless steel tube with liquid nitrogen. The direction of flow is downward (with gravity) through the tube. Heat transfer correlations for film, transition, and nucleate boiling, as well as critical heat flux, rewetting temperature, and the temperature at the onset of nucleate boiling were used to model the convection to the tube wall. Chilldown curves from the simulations were compared with data from 55 recent liquid nitrogen chilldown experiments. With these new correlations the simulation is able to predict the time to rewetting temperature and time to onset of nucleate boiling to within 25% for mass fluxes ranging from 61.2 to 1150 kg/m^{2}s, inlet pressures from 175 to 817 kPa, and subcooled inlet temperatures from 0 to 14 K below the saturation temperature.

Nomenclature

A_{CS}	=	cross-sectional area of tube material
C_p	=	specific heat at constant pressure
D	=	inner diameter of tube
F	=	two-phase Reynolds number factor
G	=	mass flux
h	=	heat transfer coefficient
k	=	thermal conductivity
Nu	=	Nusselt number, hD/k
P	=	pressure
Pr	=	Prandtl number, $C_p\mu/k$
$q_{,}$	=	heat rate
q''	=	heat flux
Re	=	Reynolds number, GD/μ
S	=	suppression factor
t	=	time
t_{tube}	=	tube thickness
T	=	temperature
T_{ONB}	=	temperature at onset of nucleate boiling
T_w	=	wall temperature

[1] Graduate Assistant, Department of Mechanical and Aerospace Engineering, University of Florida, Gainesville, FL, 32611, Student Member.
[2] Graduate Assistant, Department of Mechanical and Aerospace Engineering, University of Florida, Gainesville, FL, 32611, Student Member.
[3] Graduate Assistant, Department of Mechanical and Aerospace Engineering, University of Florida, Gainesville, FL, 32611, Student Member.
[4]Professor, Department of Mechanical and Aerospace Engineering, University of Florida, Gainesville, FL, 32611
[5] Research Aerospace Engineer, Propellants and Propulsion Branch, 21000 Brookpark Road, Cleveland, OH 44135, Senior Member.
[6]Aerospace Technologist, Thermal and Combustion Analysis Branch, Mail Stop ER43, Senior Member.

T_{wet} = rewetting temperature
We = Weber number, $G^2D/(\rho\sigma)$
x_e = equilibrium quality
X_{tt} = Martinelli parameter, $[(1 - x_e)/x_e]^{0.9}(\rho_v/\rho_l)^{0.5}(\mu_l/\mu_v)^{0.1}$
z = distance downstream of inlet
Δt = time step
Δz = node spacing
γ = enthalpy
θ = nondimensional temperature
μ = dynamic viscosity
ρ = density
σ = surface tension
σ_{SB} = Stefan-Boltzmann constant

Subscripts

conv = convection to the wall from inside fluid
CHF = critical heat flux
data = from data measurements
D = with respect to inner diameter
DB = Dittus-Boelter
f = fluid
fb = film boiling
i = node number
l = liquid property at saturation temperature
L = with respect to length downstream of inlet
nb = nucleate boiling
parasitic = parasitic heat
s = solid tube wall
sat = saturation property
sim = from the simulation
tb = transition boiling
v = vapor property at saturation temperature
w = wall

I. Introduction

The use of cryogenic propellants in chemical rocket engines like liquid oxygen (LOX) and liquid hydrogen (LH_2) is desirable because cryogens are non-toxic and have a higher specific impulse compared to other propellants. LH_2 is also used to power nuclear rocket engines which have a significantly higher specific impulse than any chemical propellant combination. On the other hand, the transfer of a liquid cryogen is much more difficult than the transfer of storable propellants (propellants that maintain a liquid phase at normal temperatures like RP-1 and hypergols) in terms of both safety and efficiency. The transfer of storable propellants from a tank to an engine or receiver tank is trivial in comparison to the transfer of cryogenic propellants. Cryogens are stored at extremely low temperatures, and when they are introduced to a normal temperature transfer line they immediately absorb heat from the tube and proceed to boil. This is problematic in most cases since the transfer of vapor-free propellant is critical, like in the case of transferring propellant from a propellant storage tank to another tank, engine, or a fuel depot. Some quantity of the cryogen must be used to chill down the tube before single-phase liquid can be transferred through the entire line. The amount that is used is dependent on the flow rate and heat flux from the tube wall to the fluid.

Unfortunately, the robust, accurate prediction of two-phase flow boiling heat transfer continues to be a challenge. The diversity of two-phase flow features that occur during chilldown makes it a complex task to provide correlations that are valid over a wide range of conditions. Typically, separate heat transfer correlations are used for different boiling regimes and sometimes different flow patterns. It is vital for designers of cryogenic propellant feed

systems both on the ground and in microgravity that robust heat transfer correlations are provided to enable accurate predictions of the chilldown process.

This paper presents an experimentally validated one-dimensional (1D) numerical simulation of the chilldown of a vertically-aligned tube with liquid nitrogen (LN_2) using a new set of two-phase flow boiling heat transfer correlations. Brief summaries are first given on the chilldown process with a focus on the different boiling regimes, previous cryogenic chilldown models, and the experiment from which the data is used to validate the heat transfer correlations used in the current work. Then the heat transfer correlations used in the simulation are described for each boiling regime and a description is given on the setup of the numerical simulation. Lastly, the results of the simulation are compared to the data. The success of this simulation demonstrates that these correlations can be integrated into any one-dimensional, one-fluid model to enable the accurate and economical prediction of transfer line chilldown.

II. Cryogenic Chilldown Process

The cryogenic chilldown process can be perceived as a reverse boiling curve, which divides the boiling process into three different regimes.[1,2] Data from a LN_2 chilldown test at an average mass flux of 39 kg/m^{2}s and average pressure of 202 kPa is shown in Figure 1, which consists of a temperature vs. heat flux plot on the left and a temperature vs. time plot on the right. At the start of the transfer, the tube is at such a higher temperature (between 270 K and 300 K depending on the ambient conditions) than the saturation temperature of the cryogen (between 77 K and 110 K for LN_2 depending on the fluid pressure) that any liquid approaching the wall is vaporized, leaving only vapor touching the wall. This is called film boiling and it persists for a majority of the chilldown time. Only once the temperature of the wall drops below the rewetting temperature (about 120 K for the test in Figure 1) does a significant amount of liquid begin to touch the wall. This rewetting temperature is called the Leidenfrost temperature for droplet vaporization experiments. This marks the initiation of transition boiling, which consists of unpredictable, intermittent intervals of liquid-to-wall contact and vapor-to-wall contact. Transition boiling can be seen as the mixture of film boiling and nucleate boiling. The heat flux increases as the temperature drops further below the rewetting temperature until the critical heat flux (CHF) is reached, which marks the start of full nucleate boiling. During nucleate boiling, liquid remains in contact with the wall while vapor bubbles or slugs still subsist within the flow. The CHF is usually the largest amount of heat flux during the entire chilldown process, and as the temperature of the tube wall continues to decline, the heat flux decreases until all bubbles are condensed. If the temperature of the incoming liquid is below the temperature at the onset of nucleate boiling (ONB), there is not enough superheat to sustain nucleate boiling. Single-phase convection heat transfer between the wall and the liquid is the only mode of heat transfer left. Typically the ONB occurs between 5 K and 10 K above the saturation temperature for LN_2.[3]

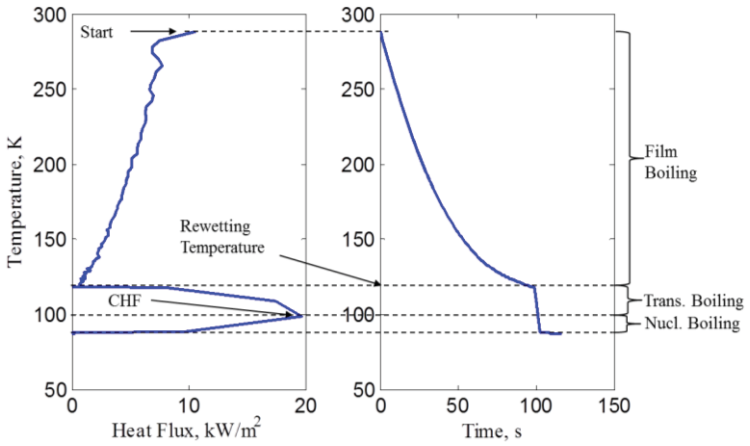

Figure 1. Typical chilldown curve for a single test. *Temperature vs. heat flux plot on the left, temperature vs. time plot on the right. The different boiling regimes are shown.*

Prediction of the heat flux during the chilldown process is a difficult task because it depends on the mass flux, the fluid properties, the tube properties, the amount of gravity, the direction of flow with respect to gravity, and even the surface finish of the tube, among other things. Additionally, chilldown is a transient process with a degree of unpredictability due to the instabilities of two phase flows and the complicated interaction at the solid-liquid-vapor interface. To achieve the best accuracy, heat transfer coefficient (HTC) correlations are provided separately for each boiling regime to predict the heat transfer from the wall to the fluid. Moreover, models for the rewetting temperature, the CHF, and the ONB temperature are required to determine the dividing points between regimes.

III. Other Chilldown Models

Many previous simulations of the cryogenic chilldown of tubes have only used one HTC correlation for all three boiling regimes. For example, Cross et al.,[4] Majumdar and Steadman, [5] and Majumdar and Ravindran[6] each used the modified Miropolskii correlation for all two-phase flow conditions. [7] This worked well for predicting chilldown rates with hydrogen at high flow rates in long transfer lines (about 60 m). The correlation, however, does not work well for other fluids like LN_2 where there is a clear presence of three distinct boiling regimes. Nor does it work well for situations of nonequilibrium and flow instability, which occur frequently in cryogenic flow systems. Nonequilibrium in flow boiling typically occurs in two situations. One is when subcooled liquid is introduced into a tube at relatively high mass fluxes in which the tube temperature is higher than the rewetting temperature. In this situation a vapor annulus at the saturation temperature surrounds a subcooled liquid core. Because the two phases of the fluid are at different temperatures the system is said to be in thermal nonequilibrium. Calculating the equilibrium quality based on the enthalpy can lead to a negative value. The second situation of nonequilibrium occurs in high quality flow in which the vapor becomes superheated even with the presence of liquid droplets that are at the saturation temperature. Calculating the equilibrium quality based on the enthalpy can lead to a value greater than one.

Agrawal et al.[8] simulated the chilldown of a tube with LN_2 using a separate correlation for film boiling and nucleate boiling. The Miropolskii correlation was used for film boiling and the Chen correlation was used for nucleate boiling. Again, nonequilibrium situations could not be modeled by using the Miropolskii correlation. It was not specified what was used for transition boiling. The predicted wall temperatures were not compared to data. Yuan et al.[9] developed a two-fluid model for film boiling and used the Chen correlation for both transition and nucleate boiling. The two-fluid model required solving two sets of conservation equations for the fluid with several semi-empirical closure models. The model worked well against data and took into account nonequilibrium, but required careful attention to the numerical solution procedure and very small time stepping to ensure stability and accuracy. Accurate correlations that can be applied to a more efficient one-fluid model, but do not sacrifice the ability of predicting the heat flux in nonequilibrium conditions, like the correlations of the current work, would be preferred over this approach for a 1D, one-fluid model simulation. The correlation set presented in this paper goes further than other one-fluid cryogenic chilldown models by:

- applying a new film boiling heat transfer correlation that is usable in nonequilibrium conditions
- applying a separate correlation for transition boiling
- giving explicit correlations for CHF, rewetting temperature, and the ONB temperature to allow easy coding logic to determine which HTC correlation to use

IV. Chilldown Experiment Overview

LN_2 chilldown experiments were designed, built, and performed at the University of Florida Department of Mechanical and Aerospace Engineering in Gainesville, FL. The purpose of the experiment was to obtain chilldown curves on a vertically aligned stainless steel tube with a downward flow direction over a wide range of mass flow rates and pressure conditions in order to support the development of robust heat transfer correlations in each of the three boiling regimes. LN_2 was selected as the test fluid in the present study not only for the safety consideration but also because its properties such as the surface tension, boiling point and evaporative latent heat are similar to those of LOX. The initial temperature of the test section was kept at normal room temperature, near 293 K, for all the runs.

The tests were operated as follows: At the start, the hardware leading up to the test section was pre-chilled by flowing LN_2 from a pressurized gas cylinder from the cryogenic Dewar through a subcooling pool cooler and eventually to vent. The subcooling pool cooler gave a subcooling margin between 0 and 14 K at the bypass valve just before the test section. After the line upstream of the test section was completely chilled down, which was verified by a TC embedded in the flow just upstream of the bypass valve, the three-way bypass valve was opened to allow flow into the test section. The test section was housed inside a stainless steel chamber which provided a vacuum environment of 0.014 Pa pressure to insulate the test section. The transient temperature and pressure data along the tube were collected by T-type thermocouples (TCs) and pressure transducers (PTs). Downstream of the test section, the two-phase flow entered a heat exchanger, where the two-phase flow fully evaporated into warm nitrogen vapor, which enabled a single-phase flow rate measurement with a gas flow rate meter. The test was terminated once the temperature readings on the test section showed that the temperature had dropped well below the ONB temperature and maintained a steady condition.

Figure 2 shows a schematic of the test section (rotated 90° counterclockwise), which is a 57.2 cm long, 1.27 cm outside diameter, 0.0508 cm thick stainless steel tube. For each test, single-phase LN_2 was supplied to the test section inlet (just downstream of the bypass valve), at a certain flow rate and pressure. The vacuum chamber was used to remove most of the surrounding air in the test section and thus significantly reduced the amount of heat transfer from the ambient environment to the tube. This lessened the uncertainty in determining the convective heat flux between the inner wall of the test section and the fluid. A set of three TCs was placed at two axial locations on the test section inside the vacuum chamber. TC-1, 2, and 3 were located upstream of TC-4, 5, and 6. The TCs were attached to the outer tube wall and placed 90° apart around the tube circumference. Two PTs, PT-1 and PT-2, were also placed inside the test section 3 cm apart from the TCs.

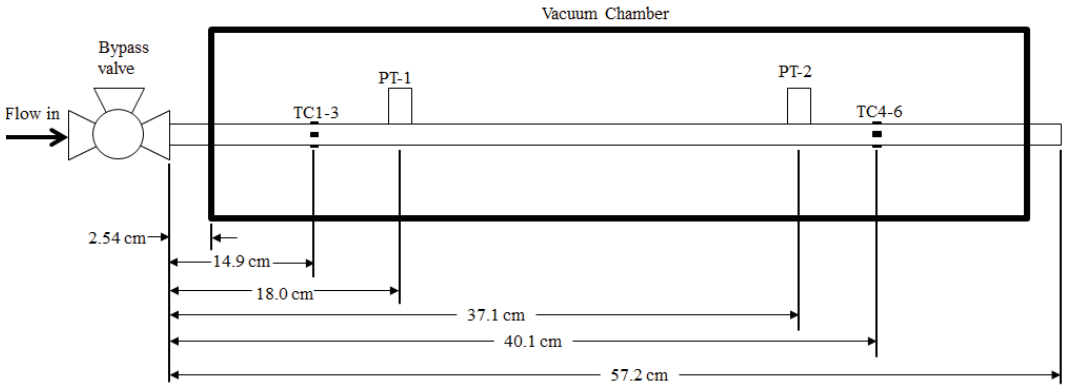

Figure 2. Test section geometry. *TC-1, TC-2, and TC-3 are the three thermocouples that make up the upstream TC station. TC4-6 make up the downstream TC station. PT-1 and PT-2 are the upstream and downstream pressure transducers, respectively. The bold black box represents the vacuum chamber.*

V. Heat Transfer Correlations

In this section each HTC correlation for the three boiling regimes is presented, along with correlations for the rewetting temperature, the CHF, and the ONB temperature. These correlations are used in the chilldown simulation presented in the following sections.

A. Film Boiling HTC Correlation

A major portion of LN_2 chilldown is spent in film boiling.[1,2] During film boiling, the flow features can change depending on the mass flux, the distance from the tube inlet, etc. For an intermediate to high mass flux a liquid core can penetrate from the quenching front to a long distance downstream. The vapor forms an annulus around the liquid so that there is no liquid-to-wall contact. This is called inverted annular flow. For low Re numbers this core can be negligibly small or nonexistent and the film boiling regime consists of a high quality mixture where the liquid is in the form of droplets or small slugs. This type of flow is called dispersed flow. These are the two regimes of flow in film boiling. Several studies have divided these flow regimes into smaller subregimes. This paper will, however, utilize a correlation that is employed for the entire film boiling regime, regardless of the flow structure.

The correlation for the film boiling Nusselt (Nu) number, fit to all of the vertical downward flow data, is given as:

$$Nu_{fb} = h_{fb}D/k_v = \left(7.55\times10^{-4} - 7.43\times10^{-6}z/D\right)Re_v^{0.941}\left(1-x_e\right)^{-5.23}Pr_v^{0.4} + 0.0568\left(k_l/k_v\right)We_z\theta_{fb}^3 \qquad (1)$$

where $We_D = G^2D/(\rho_l\sigma)$ is based on tube diameter D, and $\theta_{fb} = (300 - T_w)/(300 - T_{wet})$ is the nondimensional film boiling temperature. The temperatures are in units of Kelvin. The subscript "v" and "l" denote that the property is a vapor property and liquid property, respectively, evaluated at the saturation temperature.

The first of the two terms in this correlation accounts for the heat transfer between the wall and the vapor. It is very similar to the single-phase Dittus-Boelter equation except that it is dependent on the distance from the inlet, and that it includes two-phase effects. The farther from the inlet, the smaller the heat transfer to the vapor which is likely a result of the developing thermal and hydrodynamic boundary layers near the inlet. The $(1 - x_e)$ term accounts for the size of the vapor layer and thus the actual speed of the vapor layer. As the quality increases the vapor layer

thickens, and from continuity, the velocity of the vapor near the wall increases. The term $(1 - x_e)$ was chosen instead of including x_e inside Re_v because in the case of a subcooled inlet where x_e is negative; $(1 - x_e)^{-5.23}$ produces a real number, but including a negative x inside Re_v would produce an imaginary number when taken to the power of 0.941. Pr_v accounts for the differences between fluids. The exponent is left as 0.4 to match the single-phase Dittus-Boelter equation.

The second term in Eq. (1) represents the added heat transfer from liquid impingement against the wall. The breakup of the liquid core and subsequent two-phase mixing can be so violent that it causes liquid slugs or droplets to eject from the liquid core and impinge on the wall and vaporize, effectively increasing the heat flux from the wall. This effect is more significant for higher mass fluxes. It has been shown that the breakup of the liquid core is a strong function of the We number.[10-12] From the current work it was estimated that the added heat transfer from this effect increases linearly with We number. It was also determined from analyzing the data that the liquid impingement effect increases nonlinearly with θ_{fb}. θ_{fb} goes to zero at T_w = 300 K. (The constant in θ_{fb} was chosen as 300 K instead of the test starting temperature of 293 K because it was a round number to base the correlation on. In this case when T_w is 293K θ_{fb} is still almost zero and can be considered negligible.) For T_w > 300 K, θ_{fb} should be set to zero, although it would be wise for the user to validate the correlation at temperatures above this temperature. As T_w is lowered θ_{fb} increases, matching the trend that lowering the wall temperature increases the liquid impingement effect. The physical reasoning for this is that as the wall temperature is lowered, there is less production of vapor at the surface to resist the momentum of the liquid droplets approaching the wall. At lower values of T_w, more droplets are able to penetrate the vapor film and make contact with the tube surface, effectively increasing the heat flux beyond normal film boiling values. θ_{fb} is a maximum value of 1 at $T_w = T_{wet}$. For wall temperatures below T_{wet} the correlation is no longer used because the flow has entered transition boiling. It was estimated that a power of 3 for θ_{fb} was appropriate.

B. Nucleate Boiling HTC Correlation

Many correlations in the literature for flow boiling in the nucleate boiling regime utilize the boiling (Bo) number $Bo = q''/(G\gamma_{lv})$.[13-17] These correlations are based on steady-state heated tube data with the main application of electronics cooling or controlled heating where the heat flux is applied and known. In these cases the variable of interest is the wall superheat, i.e. how hot the tube wall material will get for a known heat flux and known mass flux of the liquid. In chilldown, the heat flux is the variable of interest, or the unknown variable. The wall superheat is the known variable since it is known at each time step of the simulation. If one were to use one of the many correlations in the literature with the Bo number as one of the parameters then this would require iteration until the heat flux on the LHS of the equation matched the heat flux on the RHS. This has the potential of significantly slowing down the simulation run time. Additionally, it has been shown that the transient nature of quenching (i.e. chilldown) data causes it to deviate from steady-state data.[18]

Therefore the approach taken in the current work is to find a correlation that is a function of all the variables that are known, e.g. the mass flux, the fluid and wall properties, etc. The correlation developed by Chen[19] provides the base form for a very robust correlation. It is based on the physics of the heat transfer process and thus does not involve an empirical correlation in terms of the Bo number. The Chen correlation will be described here.

The nucleate boiling regime HTC, h_{nb}, is the sum of the HTC responsible for forced convection with the two-phase fluid, h_{fc}, and the HTC responsible for the heat transfer that arises from bubble nucleation and growth in surface cavities, h_b. The former is sometimes called macroconvection whereas the latter is called microconvection. The equation for h_{nb} is:

$$h_{nb} = h_{fc} + h_b \tag{2}$$

where the two components are:

$$h_{fc} = 0.023\left[Re_l\left(1-x_e\right)\right]^{0.8} Pr_l^{0.4}\frac{k_l}{D}F \tag{3}$$

$$h_b = 0.00122\frac{k_l^{0.79}C_{p,l}^{0.45}\rho_l^{0.49}}{\sigma_l^{0.5}\mu_l^{0.29}\gamma_{lv}^{0.24}\rho_v^{0.24}}\left[T_w - T_{sat}\left(P\right)\right]^{0.24}\left[P_{sat}\left(T_w\right) - P\right]^{0.75}S \tag{4}$$

All fluid properties are calculated at the saturation temperature. Eq. (3) is just the single-phase liquid HTC from the Dittus-Boelter equation with the factor F to account for the difference between the liquid Reynolds (Re) number and the actual two-phase Re number. The difference between the two-phase thermal conductivity and the liquid thermal conductivity are considered negligible since $k_l >> k_v$. Also the two-phase Prandtl (Pr) number is taken simply as the liquid Pr number since both Pr_l and Pr_v are typically very close for most fluids. F was found empirically by Chen as:

$$F = \left(\frac{1}{X_{tt}} + 0.213 \right)^{0.736} \tag{5}$$

The empirical term S in Eq. (4) accounts for the difference in the actual superheat and total superheat seen by bubbles growing from surface cavities. The difference is caused by the presence of the thermal boundary layer. S was found by Chen to be:

$$S = \frac{1}{1 + 2.53 \times 10^{-6} Re_l^{1.17} F^{1.4625}} \tag{6}$$

Eqs. (2)-(6) represent the correlation used by this current work to determine the HTC in the nucleate boiling regime.

C. Transition Boiling HTC Correlation

Transition boiling consists of a mix of film and nucleate boiling, it was thought that the correlation could use either or both of the film boiling and nucleate boiling correlations with an additional empirical constant. Since nucleate boiling is an order or two magnitude greater than film boiling, a fit was applied to the data with the Chen correlation HTC and the nondimensional temperature, $\theta_{tb} = (T_{wet} - T_w)/(T_{wet} - T_{sat})$. The final equation for the transition boiling HTC was:

$$h_{tb} = 0.523 \theta_{tb}^{0.390} h_{nb} \tag{7}$$

The nondimensional temperature θ_{tb} is always between 0 and 1. Hence, in transition boiling the heat transfer is only a fraction of the full nucleate boiling heat transfer because there is some presence of film boiling. When T_w is larger than T_{wet} there is no nucleate boiling yet and only film boiling. As T_w decreases below T_{wet}, θ_{tb} becomes nonzero and grows larger, indicating more nucleate boiling heat transfer is present.

D. CHF Correlation

The CHF has been reported to be a strong function of the We number based on the length downstream of the inlet.[20] The following correlation that agreed well with the data was used in the current work:

$$q''_{CHF} = 0.0527 G \gamma_{lv} We_z^{-0.2894} \tag{8}$$

where $We_z = G^2 z/(\rho_l \sigma)$.

E. Rewetting Temperature Correlation

The model developed by DeSalve and Panella[21] is used to predict the rewetting temperature. It calculates the rewetting temperature as:

$$T_{wet} = T_{sat}(P) + 0.29 d^{-1} \left[T_{MS} - T_{sat}(P) \right] \left(1 + 0.279 G^{0.49} \right) \tag{9}$$

where d = exp[3.06×10^6/($k_s \rho_s C_{p,s}$)]erfc[1751.5($k_s \rho_s C_{ps}$)$^{0.5}$] takes into account the effect of the contact temperature between the liquid and the solid. T_{MS} is the theoretical maximum superheat calculated from Spiegler et al.[22]:

$$T_{MS} = 0.844 T_{cr} \tag{10}$$

where T_{cr} is the critical temperature of the fluid in Kelvin. Both models are also described in Carbajo.[23]

F. ONB Temperature Correlation

A simple empirical fit to the data was used to correlate the ONB temperature:

$$T_{ONB} = T_{sat}(P) + 0.0071P + 5 \tag{11}$$

Again, the temperature is in Kelvin. This correlation is more empirical and likely less applicable to other fluids than one would hope. Therefore future work for this group will include developing a much more robust correlation for T_{ONB}. Eq. (11) will suffice for this paper since the main goal here is to show the importance of the accuracy of the other more robust correlations for T_{wet}, h_{fb}, h_{nb}, h_{tb}, and the CHF.

VI. 1D Simulation Description

The simulation of the chilldown of the test section tube was developed in MATLAB®. The test section, (geometry shown in Figure 2) was divided into lumped-parameter nodes and the finite volume technique was used to solve the transient energy equation in the axial direction. It was assumed that the temperature gradients in the radial and azimuthal directions were negligible in comparison to the gradients in the axial direction. This is appropriate for thin tubes like the one used in the current work. Under this assumption, the energy equation for the solid tube becomes:

$$\rho_s C_{p,s} \frac{\partial T_w}{\partial t} = k_s \frac{\partial^2 T_w}{\partial z^2} + q''_{conv}(z) + q''_{parasitic}(z) \tag{12}$$

where the subscript "s" refers to a property of the solid tube. There were two external heat fluxes: one from the fluid convection, q''_{conv}, and another from parasitic heat, $q''_{parasitic}$. Radiation and gas conduction from the surroundings outside the test section tube made up the parasitic heat and were estimated for the simulation. A central difference scheme was used for the second-order spatial derivative and the first-order fully-implicit Euler method was used for time integration. Using $m = \rho A_{cs} \Delta z$, $q''_{conv} = h_{conv}(T_f - T_w)$, and the fact that the convective heat flux acted over the inside surface of the tube and the parasitic heat flux acted over the outside surface of the tube, Eq. (12) for each node i becomes

$$mC_{p,s}\left(T_{w,i}^{j+1} - T_{w,i}^{j}\right) = \left(k_s A_{cs} \Delta t / \Delta z\right)\left(T_{w,i+1}^{j+1} - 2T_{w,i}^{j+1} + T_{w,i-1}^{j+1}\right) + \pi D \Delta z \Delta t h_{conv}\left(T_{f,i} - T_{w,i}^{j+1}\right) + \pi(D + 2t_{tube})\Delta z \Delta t q''_{parasitic} \tag{13}$$

Where j and $j+1$ represent the old and new times, Δt is the time step, Δz is the node length, m is the mass of each node, t_{tube} is the thickness of the tube, $A_{cs} = \pi/4[(D + 2t_{tube})^2 - D^2]$ is the cross-sectional area of the tube, and T_f is the fluid temperature. Figure 3 illustrates Eq. 10 for node i. Note that each solid node consists of the entire cross section and therefore envelopes the interior fluid node.

The parasitic heat flux was a summation of the heat flux due to the conduction between the thin gas in the vacuum chamber and the tube outer surface, q''_{gc}, and the heat flux due to radiation between the vacuum chamber inner surface and the tube outer surface, q''_{rad}. For two concentric cylinders with a gap in between filled with motionless air, the air having thermal conductivity of K_e, the equation for q''_{gc} becomes:

$$q''_{gc} = K_e\left(T_{w,vac} - T_w\right)\left\{\cosh^{-1}\left[\frac{(D_{vac})^2 + (D + t_{tube})^2}{D_{vac}(D + t_{tube})}\right]\left(\frac{D + t_{tube}}{2}\right)\right\}^{-1} \tag{14}$$

where $T_{w,vac}$ is the temperature of the vacuum chamber taken as a constant 293 K value, and D_{vac} = 6.02 cm is the inner diameter of the vacuum chamber. The thermal conductivity of air is a strong function of the pressure and is estimated by:[24]

$$\frac{K_e}{K_o} = \left\{ 1 + \frac{cT_{amb}}{P_{vac}\left[D_{vac} - \left(D + t_{tube} \right) \right]} \right\}^{-1} \tag{15}$$

where K_o is the thermal conductivity of air at atmospheric pressure which is approximately 26.3 mW/mK, P_{vac} is the vacuum pressure which was held at 14 Pa, T_{amb} is the ambient temperature taken as 293 K, and c is a constant equal to 7.6×10^{-5} with units of $Nm^{-1}K^{-1}$. The q''_{rad} portion is estimated by an equation describing the radiation heat flux between two infinitely long concentric cylinders:

$$q''_{rad} = \frac{\sigma_{SB}\left(T_{w,vac}^4 - T_w^4 \right)}{\frac{1}{\varepsilon_{w,tube}} + \frac{\left(1 - \varepsilon_{w,vac} \right)}{\varepsilon_{w,vac}} \left(\frac{D + t_{tube}}{D_{vac}} \right)} \tag{16}$$

where σ_{SB} is the Stefan-Boltzmann constant, $\varepsilon_{w,tube}$ is the emissivity of the tube, and $\varepsilon_{w,vac}$ is the emissivity of the vacuum chamber. The emissivity for each surface was estimated as 0.45 since both are stainless steel.

Eq. 10 was solved simultaneously for all nodes by forming a tridiagonal matrix and solving by the Thomas algorithm. For each test, the test section was discretized into 40 nodes. With a test section length of 57.2 cm, this gave a node spacing of Δz = 1.34 cm. This node spacing and a time step of Δt = 0.01 s were found to be small enough to achieve convergence. The boundary conditions were as follows. The first node, located at the test section inlet, was assumed to start and remain at the inlet liquid temperature, determined from a TC placed just upstream of the bypass valve (see Figure 2). The last node was assumed to have the same heat flux as the node prior to it. It should be noted that different boundary conditions than these were attempted but did not significantly change the results of the simulation. This is because the convective heat flux with the fluid dominated over the conduction between nodes for the entire test except after the ONB temperature. Also, the last node was several nodes downstream of the locations of interest, which are TC-1 and TC-2 in Figure 2. Initially, all nodes except the first node were set to the first temperature reading of the given test, which was typically around 293 K.

This simulation modeled the energy equation of the solid. The model assumed a constant mass flow rate and time-independent pressure distribution of the fluid during the chilldown process, and therefore the momentum and continuity equations for the fluid did not need to be solved. In reality there were some oscillations in mass flow rate and pressure for each test. An average value of the mass flow rate data was used to simulate a given test. The pressure drop through the test section was assumed to be linear. The two time-averaged pressure readings from PT-1 and PT-2 shown in Figure 2 were used to calculate a linear pressure drop along the test section. The average mass flow rate and fluid pressure found from each test were used in evaluating h_{conv}. The fluid temperature and quality, however, had to be found at each time step and each node. The method used can be described by referring to Figure 3. Next to each solid node there is a contiguous fluid node. At each time step the enthalpy of a fluid node, γ_i, was calculated by:

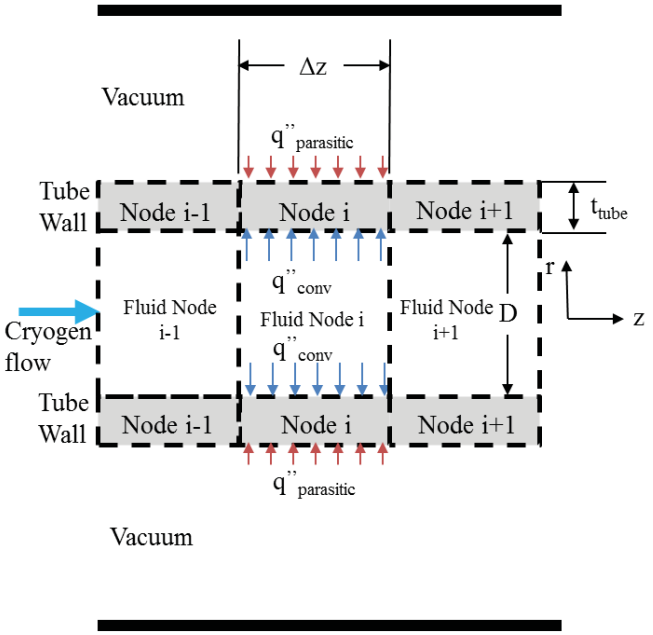

Figure 3. Numerical Simulation Setup.

$$\gamma_i = \gamma_{i-1} + q_{conv,i-1}\left[4/\left(\pi D^2 G \right) \right] \tag{17}$$

where γ_{i-1} and $q_{conv,i-1}$ are the enthalpy and the heat input in the previous node. For the first node, the enthalpy was defined by the inlet temperature and inlet pressure measured just upstream of the bypass valve. With the enthalpy

defined at each fluid node, the equilibrium quality was found by $x_e = (\gamma_i - \gamma_{l,sat})/\gamma_{lv}$ where $\gamma_{l,sat}$ and γ_{lv} are the saturated liquid enthalpy and the heat of vaporization at the local pressure. The temperature was also found knowing the enthalpy and the pressure for each node. With the local temperature, quality, and pressure, all of the fluid properties were determined at each node using Refprop, which enabled the use of the HTC correlations to evaluate h_{conv} at each node.

Even though an implicit formulation was used in Eq. (13), the enthalpy of each fluid node is solved explicitly in Eq. (17). Therefore a convergence study was performed to show that the chosen time step was small enough to achieve convergence. Time step values of Δt = 0.04 s, 0.02 s, 0.01 s, and 0.005s were used to simulate the fastest chilldown run of all 55 tests. The predicted temperature traces at TC1 are shown in Figure 4 for each time step. It is difficult to distinguish the difference between the chilldown curves, indicating an acceptable level of convergence. For further measure, the L^2 norm of the errors for Δt = 0.04 s, 0.02 s, and 0.01 s were found by assuming the Δt = 0.005 s solution was exact. The results are shown in Table 2. When changing from Δt = 0.02 s to Δt = 0.01 s the L^2 norm decreases by a much larger fraction than when changing from Δt = 0.04 s to Δt = 0.02 s. Therefore a value of Δt = 0.01 s was used for all simulations.

Table 1 – L^2-norm of the temperature errors

Time step, s	L^2-norm
0.04	31.6
0.02	19.0
0.01	7.4

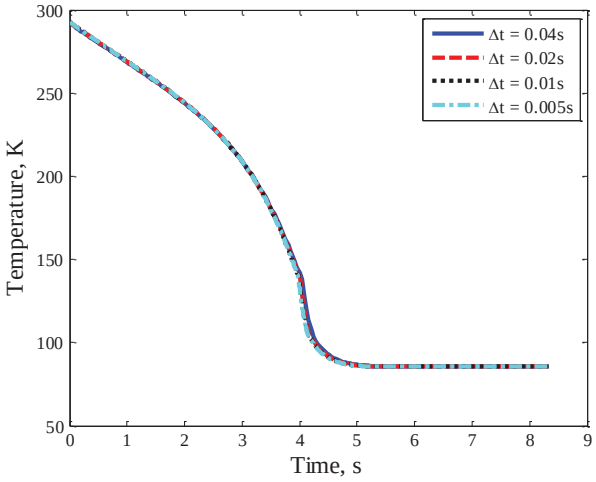

Figure 4. Predicted chilldown curves of simulation for several time step values.

The logic to determine what correlation to use – either film boiling, transition boiling, or nucleate boiling – went as follows:

- Calculate T_{wet} for the mass flow rate and local pressure
- If $T_w > T_{wet}$ then $h_{conv} = h_{fb}$
- If $T_w < T_{wet}$, then:
  - If $T_w > T_{ONB}$, then:
    - Calculate CHF
    - Calculate q''_{nb} prediction from Chen correlation
    - If $q''_{nb} > q''_{CHF}$ then $h_{conv} = h_{tb}$
    - If $q''_{nb} < q''_{CHF}$ then $h_{conv} = h_{nb}$
- If $T_w < T_{ONB}$ then $h_{conv} = h_{DB}$ where h_{DB} is the single phase Dittus-Boelter HTC

VII. Simulation Results

The simulation was run for 55 different tests with ranges of mass fluxes from 61.2 to 1150 kg/m^{2}s, inlet pressures from 175 to 817 kPa, and subcooled inlet temperatures from 0 to 14 K below the saturation temperature. Plots of the measured and predicted chilldown curves at the upstream TC stations for six different mass fluxes are shown in Figure 6-Figure 8. The mass flux, inlet liquid Re number, and inlet pressure are listed in the caption of each plot.

Table 2 – Percent MAE of temperature prediction in each boiling regime

Time Metric	MAE, s	MAPE, %
t_{wet}	4.83	24
t_{ONB}	5.15	25

As can be seen from these plots, the simulation performed well over all conditions. The main cause of the slight disagreement at all mass fluxes is likely due the simplification of using an average mass flow rate and a time-independent pressure distribution when there were actually some fluctuations in mass flux and pressure measurements for each test. An appropriate measure of the usefulness of the correlations of the current work should use the chillldown time, or how long it takes for the wall to reach the temperature of the fluid, since this is one of the main concerns from an engineering standpoint. Some of the tests were not able to reach the saturation temperature because at such low temperatures the parasitic heat began to overcome the convective heat flux, so two different time errors were considered – 1) the time from start to the rewetting temperature, t_{wet}, and 2) the time from start to the ONB, t_{ONB}. Both the mean absolute error (MAE) and the mean absolute percent error (MAPE) for t_{wet} and t_{ONB} are shown in Table 2. The two errors are defined as MAE = $1/N \times \Sigma(|t_{sim} - t_{data}|)$ and MAPE = $1/N \times \Sigma(|t_{sim} -$

$t_{data}|/t_{data}) \times 100\%$, where the subscripts t_{sim} and t_{data} stand for the time predicted by the simulation and the time measured from the data. The summation is over the N total number of data points in each regime for all 55 tests at both TC stations. Times t_{sim} and t_{data} are predicted to within 25%.

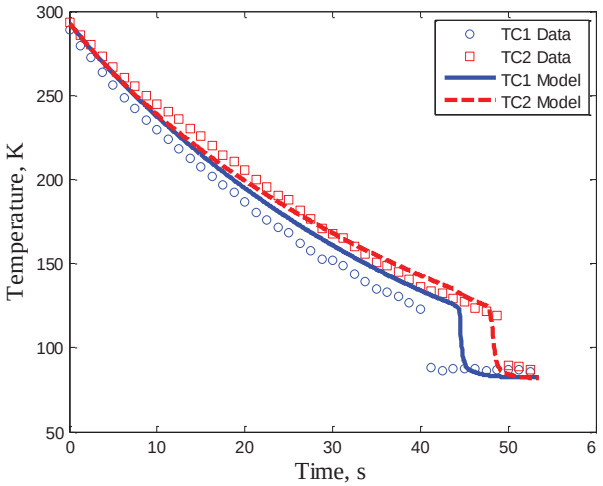

Figure 6. G = 126 kg/m^{2}s, Re_l = 11,046, P_{inlet} = 176 kPa.

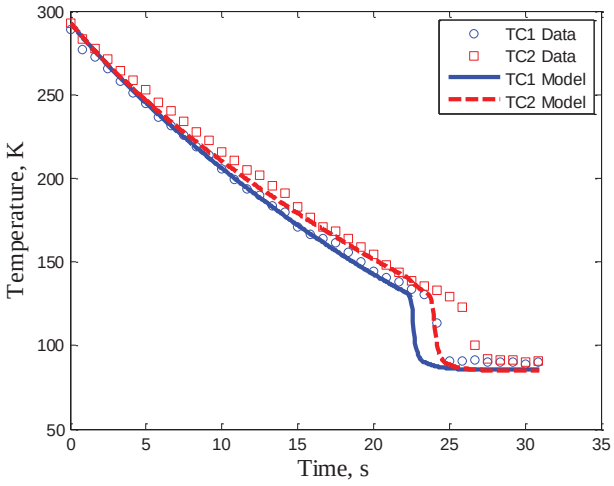

Figure 5. G = 220 kg/m^{2}s, Re_l = 21,695, P_{inlet} = 252 kPa.

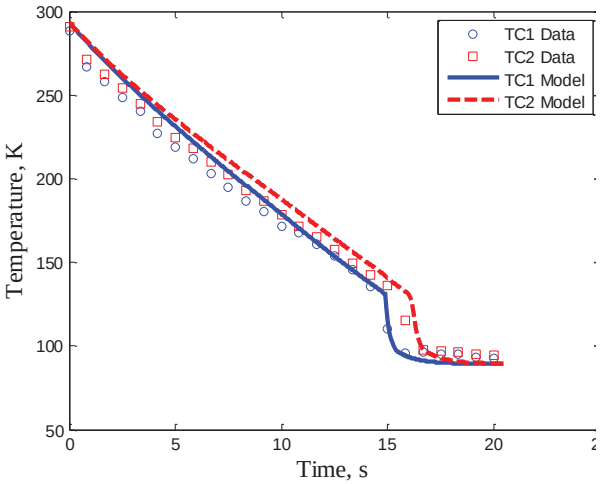

Figure 10. G = 342 kg/m^{2}s, Re_l = 37,810, P_{inlet} = 420 kPa.

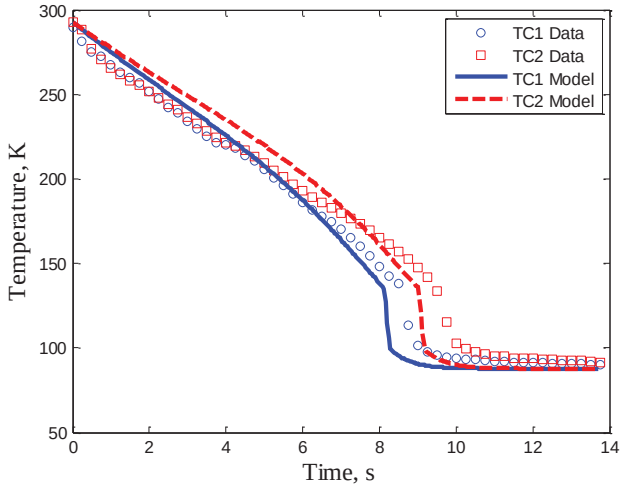

Figure 7. G = 627 kg/m^{2}s, Re_l = 65,575, P_{inlet} = 561 kPa.

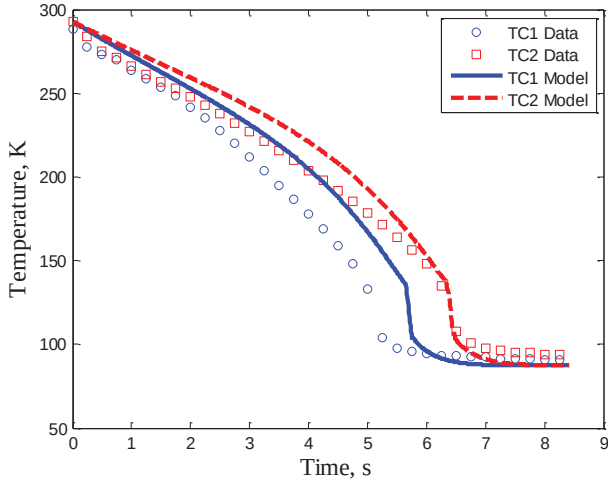

Figure 9. G = 888 kg/m^{2}s, Re_l = 91,433, P_{inlet} = 690 kPa.

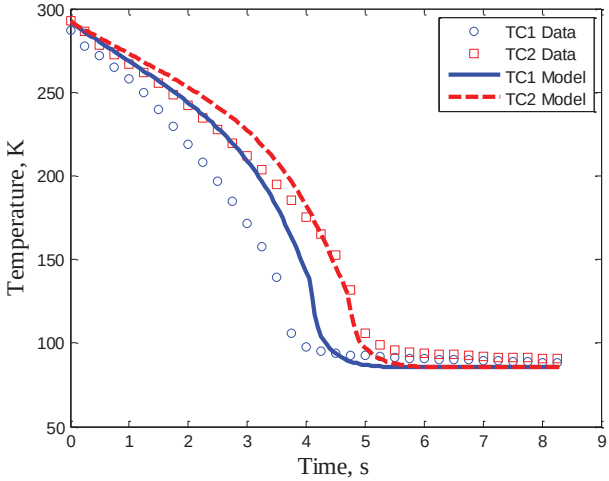

Figure 8. G = 1179 kg/m^{2}s, Re_l = 113,762, P_{inlet} = 723 kPa.

VIII. Conclusion

The numerical simulation of the chilldown of a short, thin, vertical tube with LN_2 flowing downward in the current work was able to predict the transient temperature of the tube with good agreement with the data over a wide range of conditions. These results support the validity of the HTC correlations proposed in the current work for all three of the boiling regimes (even for nonequilibrium, i.e. negative quality values, at the inlet), the correlations for the dividing points of the boiling regimes (the rewetting temperature, the CHF, and the ONB temperature), as well as the logic employed when choosing which correlation to use under local conditions. These correlations could be used to improve the accuracy of commercial simulation packages. Future work includes: a full description of the experimental apparatus and the experimental results which will include multiple flow angles in addition to the downward flow angle considered in the current work, further analysis and data comparison of the correlations in the current work, and extension of the correlations in the current work to different flow angles.

Acknowledgments

This work was funded by the NASA MSFC Space Launch System Advanced Development Project under Grant NNM13AA08G with Melinda Nettles as the Program Director.

References

[1]Hu, H., Wijeratne, T. K., and Chung, J. N., "Two-Phase Flow and Heat Transfer During Chilldown of a Simulated Flexible Metal Hose Using Liquid Nitrogen," *Journal of Low Temperature Physics*, Vol. 174, No. 5-6, 2014, pp. 247-268.

[2]Hu, H., Chung, J. N., and Amber, S. H., "An Experimental Study on Flow Patterns and Heat Transfer Characteristics During Cryogenic Chilldown in a Vertical Pipe," *Cryogenics*, Vol. 52, No. 4-6, 2012, pp. 268-277.

[3] Qi, S.L., Zhang, P., Wang, R.Z., and Xu, L.X., "Flow boiling of liquid nitrogen in micro-tubes – The onset of nucleate boiling, two phase flow instability and two phase flow pressure drop" *International Journal of Heat and Mass Transfer*, Vol. 50, 2007, pp. 4999 – 5016.

[4]Cross, M. F., Majumdar, A. K., Bennett Jr., and J. C., Malla, R. B., "Modeling of Chill Down in Cryogenic Transfer Lines," *Journal of Spacecraft and Rockets*, Vol. 39, No. 2, 2002, pp. 284-289.

[5]Majumdar, A. K. and Steadman, T., "Numerical Modeling of Thermofluid Transients During Chilldown of Cryogenic Transfer Lines," *33rd International Conference on Environmental Systems*, CP2662, Vo1. 1, SAE International, 2003.

[6]Majumdar, A. K. and Ravindran, S. S., "Numerical Prediction of Conjugate Heat Transfer in Fluid Network," *Journal of Propulsion and Power*, Vol. 27, No. 3, 2011, pp. 620-630.

[7]Miropolskii, Z. L., "Heat Transfer in Film Boiling of a Steam-Water Mixture in Steam Generating Tubes," *Teploenergetika*, Vol. 10, No. 5, 1963, pp. 49-52.

[8]Agrawal, G., Agarwal, D. K., and Kumar, S. S., " Mathematical Modeling of Cryogenic Feedline Chilldown Process," *Proceedings of the 22nd National and 11th International ISHMT-ASME Heat and Mass Transfer Conference*, ASME, New York, 2013.

[9]Yuan, K., Ji, Y., and Chung, J. N., "Numerical Modeling of Cryogenic Chilldown Process in Terrestrial Gravity and Microgravity," *International Journal of Heat and Fluid Flow*, Vol. 30, No. 1, 2009, pp. 44-53.

[10]Ishii, M. and de Jarlais, G., "Flow Regime Transition and Interfacial Characteristics of Inverted Annular Flow," *Nuclear Engineering and Design*, Vol. 95, 1986, pp. 171-184.

[11]Ishii, M. and de Jarlais, G., "Flow Visualization of Inverted Annular Flow of Post Dryout Heat Transfer Region," *Nuclear Engineering and Design*, Vol. 99, 1987, pp. 187-199.

[12]Obot, N. T and Ishii, M., "Two-phase Flow Regime Transition Criteria in Post-Dryout Region based on Flow Visualization Experiments," *International Journal of Heat and Mass Transfer*, Vol. 31, No. 12, 1988, pp. 2559-2570.

[13]Kim, S. M. and Mudawar, I., "Review of Databases and Predictive Methods for Heat Transfer in Condensing and Boiling Mini/Micro-Channel Flows," *International Journal of Heat and Mass Transfer*, Vol. 77, 2014, pp. 627-652.

[14]Liu, Z. and Winterton, R. H. S., "A General Correlation for Saturated and Subcooled Flow Boiling in Tubes and Annuli, Based on a Nucleate Pool Boiling Equation," *International Journal of Heat and Mass Transfer*, Vol. 34, No. 11, 1991, pp. 2759-2766.

[15]Gungor, K. E. and Winterton, R. H. S., "A General Correlation for Flow Boiling in Tubes and Annuli," *International Journal of Heat and Mass Transfer*, Vol. 29, No. 3, 1986, pp. 351-358.

[16]Shah, M. M., "Chart Correlation for Saturated Boiling Heat Transfer: Equations and Further Study," *ASHRAE Transactions*, Vol. 88, 1982, pp. 185-196.

[17]Ogato, H. and Sato, S., "Forced Convection Heat Transfer to Boiling Helium in a Tube," *Cryogenics*, Vol. 14, No. 7, 1974, pp. 365-380.

[18]Payayopanakul, W. and Westwater, J. W., "Evaluation of the Unsteady-state Quenching Method for Determining Boiling Curves," *International Journal of Heat and Mass Transfer*, Vol. 21, 1978, pp. 1437-1445.

[19]Chen, J. C., "Correlation for Boiling Heat Transfer to Saturated Fluids in Flow," *Industrial and Engineering Chemistry Process Design and Development*, Vol. 5, No. 3, 1966, pp. 322-329.

[20]Katto, Y. and Kurata, C., "Critical Heat Flux of Saturated Convective Boiling on Uniformly Heated Plates in a Parallel Flow," *International Journal of Multiphase Flow*, Vol. 6, 1980, pp. 575-582.
[21]De Salve, M. and Panella B., "Analytical Model for Bottom Reflooding Thermal-Hydraulics in Circular Ducts and Comparison with Experimental Results," *International Centre for Heat and Mass Transfer Seminar on Nuclear Reactor Safety Heat Transfer*, Hemisphere Publishing Corporation, Managua, Nicaragua, CA, edited by S. G. Bankoff and N. H. Afgan, 1982, pp. 742-762.
[22]Spiegler, P., Hopenfeld, J., Silberberg., M., Bumpus Jr., C. F., and Norman, A., "Onset of Stable Film Boiling and the Foam Limit," *International Journal of Heat and Mass Transfer*, Vol. 6, 1963, pp. 987-994.
[23]Carbajo, J. J., "A Study on the Rewetting Temperature," *Nuclear Engineering and Design*, Vo. 84, 1985, pp. 21-52.
[24]*Fluid Flow Databook*, General Electric, Genium Publishing, Section 410.2, May 1982.